miR-34s inhibit osteoblast proliferation and differentiation in the mouse by targeting SATB2

Jianwen Wei,[1] Yu Shi,[1] Lihua Zheng,[1] Bin Zhou,[2] Hiroyuki Inose,[1] Ji Wang,[2] X. Edward Guo,[2] Rudolf Grosschedl,[3] and Gerard Karsenty[1]

[1]Department of Genetics and Development, College of Physicians and Surgeons, Columbia University, New York, NY 10032
[2]Department of Biomedical Engineering, Columbia University, New York, NY 10027
[3]Department of Cellular and Molecular Immunology, Max Planck Institute of Immunobiology, Freiburg 79108, Germany

A screen of microRNAs preferentially expressed in osteoblasts identified members of the miR-34 family as regulators of osteoblast proliferation and/or differentiation. Osteoblast-specific gain- and loss-of-function experiments performed in vivo revealed that miR-34b and -c affected skeletogenesis during embryonic development, as well as bone mass accrual after birth, through two complementary cellular and molecular mechanisms. First, they inhibited osteoblast proliferation by suppressing Cyclin D1, CDK4, and CDK6 accumulation. Second, they inhibited terminal differentiation of osteoblasts, at least in part through the inhibition of SATB2, a nuclear matrix protein that is a critical determinant of osteoblast differentiation. Genetic evidence obtained in the mouse confirmed the importance of SATB2 regulation by miR-34b/c. These results are the first to identify a family of microRNAs involved in bone formation in vivo and to identify a specific genetic pathway by which these microRNAs regulate osteoblast differentiation.

Introduction

Our understanding of the intracellular mechanisms governing osteoblast differentiation has made significant progress in the last 15 years. Schematically, three levels of regulation have been characterized in detail.

First, there are transcription factors that are either osteoblast-specific or highly expressed in cells of the osteoblast lineage. Three factors–Runx2, Osterix, and ATF4–act sequentially to control differentiation from an osteochondral progenitor to a fully differentiated and functional osteoblast (Ducy et al., 1997; Komori et al., 1997; Nakashima et al., 2002; Yang et al., 2004). In addition, more broadly expressed transcription factors such as members of the AP1 family, CREB and FOXO1, also contribute to osteoblast differentiation and function (Kenner et al., 2004; Bozec et al., 2010; Rached et al., 2010; Kajimura et al., 2011). A second level of regulation is exerted by nuclear proteins such as STAT1, Twist, or Schnurri, among others. These factors interact with Runx2, Osterix, and/or ATF4 to decrease their activity, thereby delaying the onset of osteoblast differentiation (Kim et al., 2003; Bialek et al., 2004; Jones et al., 2006). The third level of regulation relies on proteins that are part of the nuclear matrix and bind DNA at nuclear matrix attachment regions (MARs). One such factor, SATB2, is involved in osteoblast differentiation through two distinct mechanisms. It inhibits expression of *Hoxa2*, a negative regulator of *Runx2* expression (Kanzler et al., 1998), while increasing the activity of Runx2 and ATF4 (Dobreva et al., 2006). As a result, SATB2 favors osteoblast differentiation, and thus the expression of *Osteocalcin* and *Bone sialoprotein* (*Bsp*), which can be used as molecular markers of its activity.

In the last decade, small noncoding RNAs have emerged as important regulators of gene expression. MicroRNAs (miRNAs) are small noncoding RNAs that down-regulate expression of their target genes by either mRNA degradation or translational inhibition (Valencia-Sanchez et al., 2006; Bartel, 2009; Djuranovic et al., 2011; Huntzinger and Izaurralde, 2011). Although most miRNAs are broadly expressed, some have a more restricted pattern of expression, and influence cell differentiation (Poy et al., 2004; Zhao et al., 2005; Johnnidis et al., 2008). The importance of this mode of gene regulation during skeletogenesis is inferred by the observation that inactivation of

Correspondence to Gerard Karsenty: gk2172@columbia.edu

Abbreviations used in this paper: BFR, bone formation rate; *Bsp*, *Bone sialoprotein*; ES, embryonic stem; miRNA, microRNA; qPCR, quantitative PCR; UTR, untranslated region; WT, wild type.

The Rockefeller University Press $30.00
J. Cell Biol. Vol. 197 No. 4 509–521
www.jcb.org/cgi/doi/10.1083/jcb.201201057

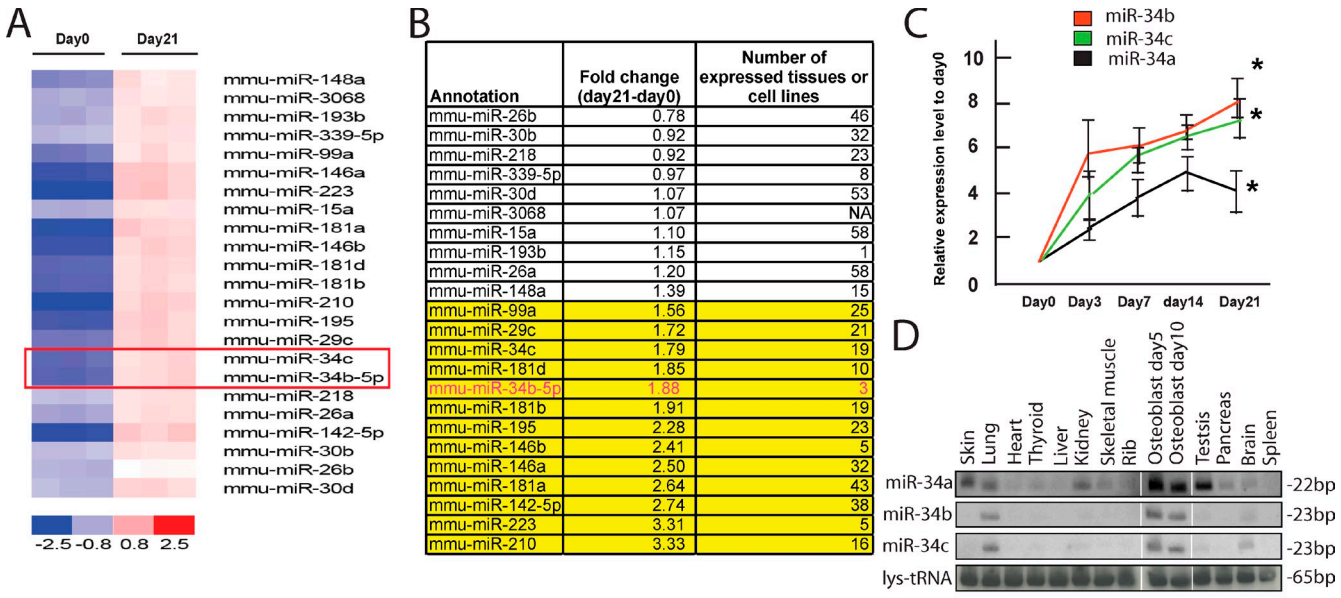

Figure 1. **Expression profile of miR-34s and the consequence of miR-34c overexpression in osteoblasts.** (A) miRNA expression profile in pre-osteoblasts (day 0) and mature osteoblasts (day 21), as determined by microarray analysis (n = 3). miR-34s are highlighted by a box. (B) Expression pattern of miRNAs increased during osteoblast differentiation. (C) Expression profile of miR-34s during osteoblast differentiation, determined by qPCR (n = 3). The asterisks indicate that the expression of miR-34s was significantly higher at day 21 than at day 0. Error bars indicate means ± standard errors of the mean. (D) Expression pattern of miR-34s, determined by Northern blotting. Tissue RNA samples were extracted from 7-d-old mice.

DICER, a protein necessary for processing of miRNAs, affects osteoblast differentiation (Gaur et al., 2010). Accordingly, it has been suggested that miRNAs may be involved in osteoblast proliferation and/or differentiation (Hassan et al., 2010; Zhang et al., 2011). However, these observations were derived from gain-of-function experiments performed in cell culture. To date, no miRNA has been shown, through cell-specific loss-of-function experiments performed in the mouse, to regulate osteoblast proliferation and/or differentiation in vivo.

We present here two miRNAs—miR-34b and miR-34c—as key regulators of skeletogenesis through two complementary mechanisms. miR-34s inhibit osteoblast proliferation by decreasing Cyclin D1, CDk4, and CDK6 accumulation while simultaneously inhibiting osteoblast differentiation by decreasing SATB2 accumulation.

Results

Identification of miRNAs differentially expressed during osteoblast differentiation

With the goal of identifying miRNAs whose expression increases during osteoblast differentiation, osteoblasts obtained from mouse calvaria were cultured in the presence or absence of differentiation medium containing β-glycerophosphate and ascorbic acid. Under these conditions, osteoblasts take 21 d to fully differentiate (Bakker and Klein-Nulend, 2003). They were then subjected to miRNA expression profile analysis, which identified a large number of miRNAs whose expression increased significantly during osteoblast differentiation (Fig. 1 A). A systematic analysis of their global pattern of expression using a published mammalian miRNA expression atlas (Landgraf et al., 2007) identified miR-34b as having the most restricted expression pattern among those miRNAs whose expression increased >1.5-fold during osteoblast differentiation (Fig. 1 B).

There are three miR-34s: miR-34a is encoded by a gene located on mouse chromosome 4, whereas miR-34b and miR-34c are encoded by genes 510 bp apart on chromosome 9. The miRNA expression profile analysis revealed a 1.8-fold increase in the expression of miR-34b and miR-34c during the course of osteoblast differentiation, whereas expression of miR-34a increased only modestly (Fig. 1 B and not depicted). This was validated by a quantitative PCR (qPCR) analysis showing that expression of miR-34b and miR-34c increased sevenfold during osteoblast differentiation, whereas miR-34a again showed a modest increase (Fig. 1 C). Moreover, miR-34a was more broadly expressed compared with miR-34b and miR-34c, whose expression was primarily restricted to osteoblasts with decreased expression observed in the brain and lung (Fig. 1 D). We also compared the spatial patterns of expression of miR-34b and miR-34c to those of miR-23a, miR-24-2, and miR-27a (Hassan et al., 2010), as well as those of miR-146b and miR-223, two additional miRNAs identified in our screen. As shown in Fig. S1 A, none of the miRNAs examined had the same restricted pattern of expression as miR-34b and -c. The relative cell specificity observed for miR-34b/c together with their induction during osteoblast differentiation gave us an incentive to study miR-34s functions in osteoblasts in vivo.

miR-34b and -c influence bone mass accrual postnatally

To determine whether miR-34s are involved in osteogenesis, we used a gain-of-function approach and generated transgenic mice overexpressing one representative member of this family,

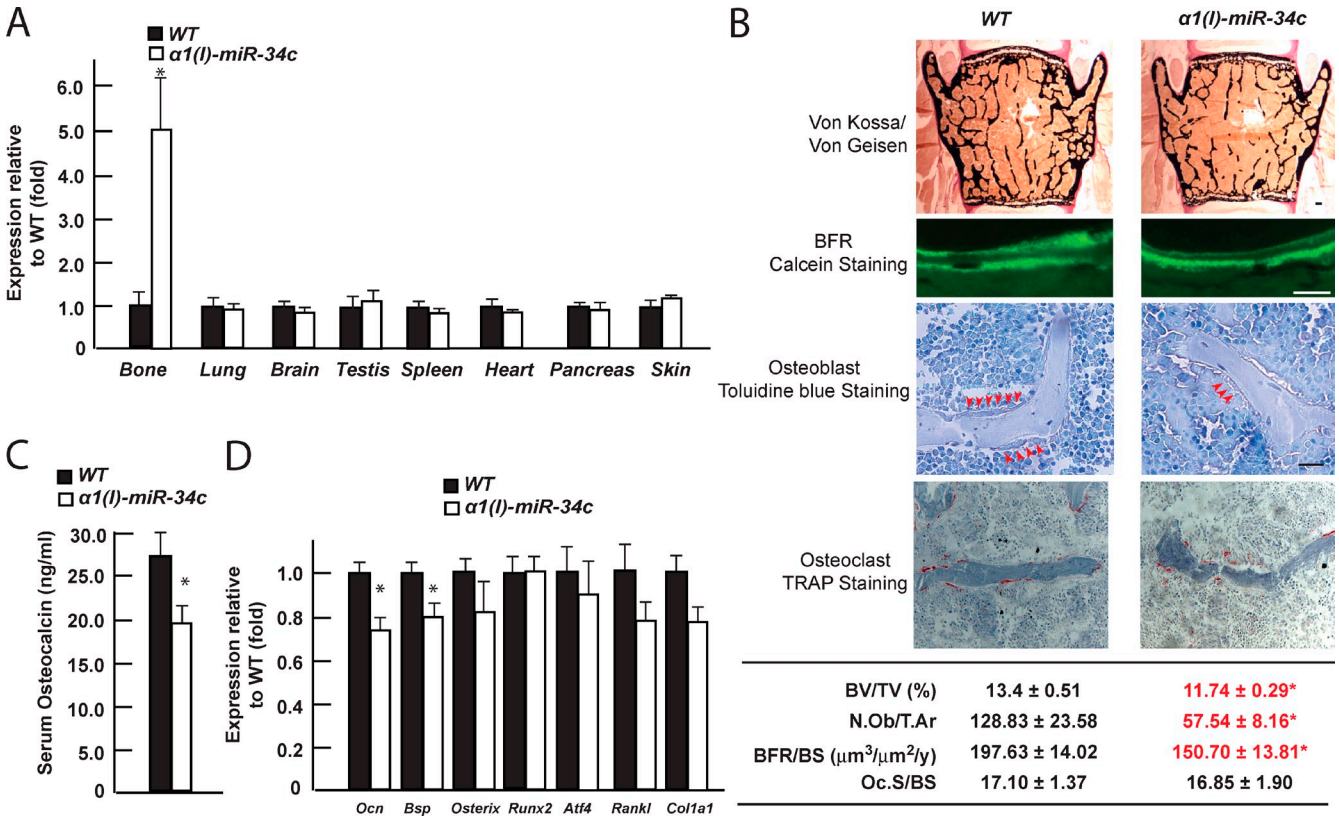

BV/TV (%)	13.4 ± 0.51	11.74 ± 0.29*
N.Ob/T.Ar	128.83 ± 23.58	57.54 ± 8.16*
BFR/BS ($\mu m^3/\mu m^2/y$)	197.63 ± 14.02	150.70 ± 13.81*
Oc.S/BS	17.10 ± 1.37	16.85 ± 1.90

Figure 2. **Overexpessing miR-34c in osteoblasts specifically decreased bone mass.** (A) Tissue expression pattern of miR-34c in *α1(I)* miR-34c transgenic mice, determined by qPCR (n = 3–5). (B) Bone histomorphometric analysis of L3 and L4 vertebrae of 3-mo-old *α1(I)* miR-34c transgenic mice (n = 5–9). Mineralized bone volume over the total tissue volume (BV/TV), as revealed by Von Kossa/Von Gesien staining; mineralized tissues were stained black and nonmineralized tissues were stained red. Osteoblast number per tissue area (N.Ob/T.Ar), as revealed by toluidine blue staining and osteoblasts (arrowheads), were identified as plump, cuboidal cells with a perinuclear clear zone on bone surfaces); the annual fractional volume of trabecular bone formed per unit trabecular surface area (BFR/BS) was calculated from the extent of bone surface labeled with calcein (fluorescent green labels) and the distance between the labels in areas where two labels are present. Osteoclast surface per bone surface (Oc.S/BS), as measured by TRAP staining; osteoclasts were identified as red staining cells on the bone surface. Bars, 20 μm. (C) Serum osteocalcin level in *α1(I)* miR-34c transgenic mice (n = 16–23). (D) Expression level of osteoblast markers in bones of *α1(I)* miR-34c transgenic mice, determined by qPCR (n = 7–8). Error bars indicate means ± standard errors of the mean. *, $P \leq 0.05$.

miR-34c, specifically in osteoblasts under control of the *α1(I) collagen* promoter.

One transgenic mouse line demonstrated a fivefold increase of miR-34c expression in osteoblasts in vivo, with no detectable ectopic expression in any of the other cell types tested (Fig. 2 A). A histological and histomorphometric analysis of vertebrae showed that 3-mo-old *α1(I)* miR-34c transgenic mice exhibited a low bone mass phenotype, as defined by a decrease of the mineralized bone volume over the total volume (BV/TV) of vertebrae (Fig. 2 B, top). This was accompanied with a decrease of both osteoblast number (N.Ob/T.Ar, osteoblast number/tissue area) and bone formation rate (BFR; BFR/BS, the annual fractional volume of trabecular bone formed per unit trabecular surface area), a measure of the activity of the osteoblasts. In contrast, osteoclast surface (Oc.S/BS, osteoclast surface/bone surface) was unaffected (Fig. 2 B). Consistent with these histological observations, circulating levels of osteocalcin, a marker of bone formation (Price et al., 1980), were decreased in *α1(I)* miR-34c transgenic mice, whereas those of C-terminal telopeptide of type I collagen (Ctx), a marker of bone resorption (Eyre et al., 1988), were unaffected (Figs. 2 C and S2). At the molecular level, expression of osteoblast marker genes *Osteocalcin* and *Bsp* were decreased by 30%, whereas expression of *Runx2*, *Atf4*, *Osterix*, and *Rankl*, genes known to be expressed earlier during osteoblast differentiation, were not altered in any significant manner in bones of *α1(I)* miR-34c mice; *Col1a1* expression was also only modestly decreased (Fig. 2 D).

These results prompted us to ask what would be the consequences of an osteoblast-specific inactivation of miR-34s. To that end, we generated floxed alleles of miR-34a and of miR-34bc (Fig. S3, A and B), and deleted all miR-34s from the cells of the osteoblast lineage (miR-34abc$^{Osb-/-}$ mice) using the *α1(I) collagen*-Cre transgenic mouse (Dacquin et al., 2002). Before analyzing these mutant mice, we assessed the degree of recombination at each of the two loci. Recombination was high at the miR-34b and -c loci, but more modest at the miR-34a locus, where it never exceeded 30% (Fig. S3 C). In view of this rather disparate efficiency of recombination, we analyzed both miR-34abc$^{Osb-/-}$ and miR-34bc$^{Osb-/-}$ mice. Both mutant mouse strains developed normally, were born at the expected Mendelian ratio, and had a normal life span, indicating that embryonic development can proceed in the absence of miR-34s expression in osteoblasts.

Histomorphometric analysis of 3-mo-old miR-34abc$^{Osb-/-}$ and miR-34bc$^{Osb-/-}$ mice demonstrated a significant increase

in bone mass as measured by BV/TV (Fig. 3, A and D). This was caused by a significant increase in the numbers of osteoblasts, resulting in an increase in the BFR, whereas osteoclast surface was not affected (Fig. 3, A and D). A microcomputer tomography analysis, performed with the goal of obtaining a three-dimensional appreciation of the bone structure, showed that cortical bone volume, bone mineral density, and cortical thickness were all increased in miR-34bc$^{Osb-/-}$ long bones (Fig. 3 E). Consistent with their increase in osteoblast number, serum levels of osteocalcin were significantly increased in miR-34abc$^{Osb-/-}$ and miR-34bc$^{Osb-/-}$ mice (Fig. 3, B and F), whereas Ctx circulating levels were unaffected (Fig. S3, D and E). Similarly, expression of markers of fully differentiated osteoblasts, such as *Osteocalcin* and *Bsp*, was increased by 40–60%, whereas expressions of genes expressed earlier during osteoblast differentiation (*Runx2*, *Atf4*, *Osterix*, and *Rankl*) were unchanged, and *Col1a1* expression was modestly increased (Fig. 3, C and G). Hence, the histological, cellular, biochemical, and molecular abnormalities noted in miR-34abc$^{Osb-/-}$ and miR-34bc$^{Osb-/-}$ mice mirrored those effects observed in mice overexpressing miR-34c in osteoblasts. Together, these two experiments indicate that miR-34b and -c are implicated in osteoblast differentiation and/or proliferation. That the phenotypes observed in either the loss- or gain-of-function models are apparent in unchallenged animals underscores the importance of this mode of regulation of bone formation.

Molecular basis of miR-34b and -c regulation of osteoblast proliferation

Next, we examined the molecular bases behind the increase in osteoblast number observed in miR-34bc$^{Osb-/-}$ mice. A TUNEL assay performed in vivo failed to detect any difference between miR-34bc$^{Osb-/-}$ and miR-34bc$^{fl/fl}$ osteoblasts (Fig. S4 A). In contrast, BrdU incorporation analysis performed in vivo showed a significant increase in the number of proliferating osteoblasts in miR-34bc$^{Osb-/-}$ versus miR-34bc$^{fl/fl}$ bones; conversely, this number was decreased in *α1(I)* miR-34c transgenic mice (Fig. 4 A). These data indicated that miR-34b and -c affect osteoblast proliferation.

In view of this data, we used an in silico approach (TargetScanMouse 5.2; www.targetscan.org) to search for regulators of the cell cycle that could be targets of miR-34s. This analysis identified Cyclin D1 as a putative target of miR-34s. The Cyclin D1 3′ untranslated region (UTR) sequence contains a highly conserved binding site for miR-34 between 1,853 and 1,859 (Fig. 4 B). Forced expression of either member of the miR-34 family in COS cells decreased the activity of the luciferase reporter gene containing the wild type (WT), but not a mutated sequence of the 3′ UTR, of *Cyclin D1* (Fig. 4 C).

Because *Cyclin D1* expression is not affected in the absence of miR-34s (Fig. S4 B), we tested whether miR-34s affect Cyclin D1 translation by performing Western blots on osteoblast extracts isolated from miR-34bc$^{fl/fl}$ bones that were infected with an adenovirus expressing *Cre* recombinase or vector alone. There was a 2.5-fold increase in Cyclin D1 protein accumulation in miR-34bc$^{-/-}$ osteoblasts (Fig. 4 D). Likewise, knockdown of miR-34b and -c in primary osteoblasts through the transfection of specific hairpin inhibitors increased Cyclin D1 protein accumulation nearly twofold (Fig. 4 E), whereas overexpression of either member of the miR-34 family decreased endogenous Cyclin D1 accumulation 33–44% (Fig. 4 F). Moreover, Cyclin D1 protein level was increased in bones of miR-34bc$^{Osb-/-}$ mice and decreased in those of *α1(I)* miR-34c mice (Fig. 4 G).

We explored further our in silico analysis using a different database (Targets and Expression, www.microrna.org) and identified Cyclin E2, Met, Cdk4, Cdk6, E2f5, and E2f3 as potential targets of miR-34b and -c (Lee et al., 2011). The 3′ UTRs of Cdk4 and Cdk6 contain predicted binding sites for miR-34 between 196 and 218, and 214 and 236, respectively (Fig. 4 H). Western blots performed using extracts from osteoblasts isolated from miR-34bc$^{fl/fl}$ bones infected with an adenovirus expressing the *Cre* recombinase showed a 2.5-fold increase in the abundance of CDK4 and CDK6 (Fig. 4 I), whereas protein levels of Cyclin E2, MET, E2F5, and E2F3 were unchanged (Fig. S4 C). More importantly, protein levels of CDK4 and CDK6 were increased nearly twofold in bones of miR-34bc$^{Osb-/-}$ mice and decreased 60–70% in those of *α1(I)* miR-34c mice (Fig. 4 J). These data, which are congruent and were obtained through the analysis of loss- and gain-of-function mouse models, identify Cdk4 and Cdk6 as two additional targets of miR-34s in osteoblasts; hence, they provide further evidence of their ability to modulate proliferation of this cell type.

Lastly, because miR-34s have been proposed to regulate canonical Wnt signaling (Kim et al., 2011), we also examined expression of the Wnt signaling target genes: *Axin2*, *Tcf1*, *Tcf3*, and *Osteoprotegerin* (*Opg*), but failed to detect any significant change in the expression of these genes in either our loss- or gain-of-function models of miR-34s (Fig. S4 D). This is consistent with the fact that miR-34b/c disruption in osteoblasts, using the same Cre driver, does not affect *Opg* expression, osteoclast differentiation, or bone resorption, all functions affected by canonical Wnt signaling in differentiated osteoblasts (Glass et al., 2005).

miR-34b and -c inhibit osteoblast differentiation during embryonic development

Next, we asked whether miR-34s affect osteoblast differentiation. This question was raised by two observations. First, when put in culture, miR-34bc$^{Osb-/-}$ osteoblasts formed 35% more mineralized nodules than control osteoblasts (Fig. 5 A). Second, during embryogenesis, miR-34b expression increased markedly from E10.5 to E16.5 in tibiae (Fig. 5 B).

To address this question in vivo, we isolated miR-34bc$^{fl/fl}$ and miR-34bc$^{Osb-/-}$ embryos at E12.5, E13.5, E14.5, and E16.5, and generated skeletal preparations that were stained with alcian blue for cartilage, and alizarin red for mineralized ECM. The earliest time point at which we could detect a phenotypic abnormality was E13.5. At that stage there was ECM mineralization, an event suggestive of bone formation, in tibiae of miR-34bc$^{Osb-/-}$ but not of control embryos (Fig. 5 C). At E14.5, ECM mineralization was now observed in lumbar and dorsal vertebrae of miR-34bc$^{Osb-/-}$ but not in control embryos.

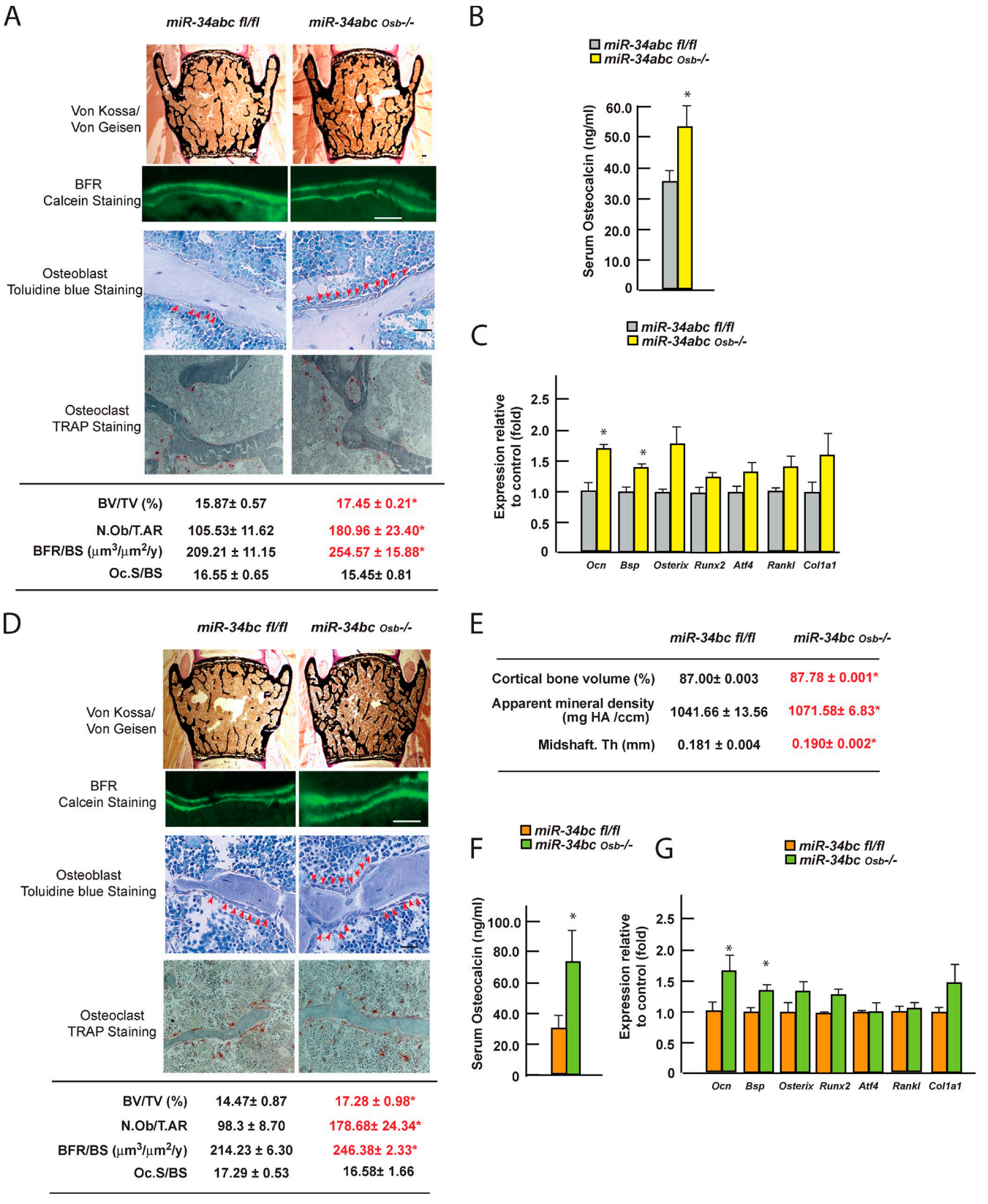

BV/TV (%)	15.87± 0.57	17.45 ± 0.21*
N.Ob/T.AR	105.53± 11.62	180.96 ± 23.40*
BFR/BS ($\mu m^3/\mu m^2/y$)	209.21 ± 11.15	254.57 ± 15.88*
Oc.S/BS	16.55 ± 0.65	15.45± 0.81

BV/TV (%)	14.47± 0.87	17.28 ± 0.98*
N.Ob/T.AR	98.3 ± 8.70	178.68± 24.34*
BFR/BS ($\mu m^3/\mu m^2/y$)	214.23 ± 6.30	246.38± 2.33*
Oc.S/BS	17.29 ± 0.53	16.58± 1.66

	miR-34bc fl/fl	miR-34bc Osb-/-
Cortical bone volume (%)	87.00± 0.003	87.78 ± 0.001*
Apparent mineral density (mg HA /ccm)	1041.66 ± 13.56	1071.58± 6.83*
Midshaft. Th (mm)	0.181 ± 0.004	0.190± 0.002*

Figure 3. **miR-34b and -c regulate bone mass accrual.** (A and D) Histomorphometric analysis of vertebrae of 3-mo-old miR-34abc$^{Osb-/-}$ (A; n = 7–12) and miR-34bc$^{Osb-/-}$ mice (D; n = 4–11). Representative histological images are shown. Bars, 20 µm. (B and F) Serum osteocalcin level in miR-34abc$^{Osb-/-}$ (B; n = 9–11) and miR-34bc$^{Osb-/-}$ mice (F; n = 11–12). (C and G) Expression level of osteoblast markers in bones of miR-34abc$^{Osb-/-}$ (C; n = 3) and miR-34bc$^{Osb-/-}$ mice (G; n = 4), determined by qPCR. (E) microCT analysis of long bones of 3-mo-old miR-34bc$^{Osb-/-}$ mice (n = 6–7). Error bars indicate means ± standard errors of the mean. *, P ≤ 0.05.

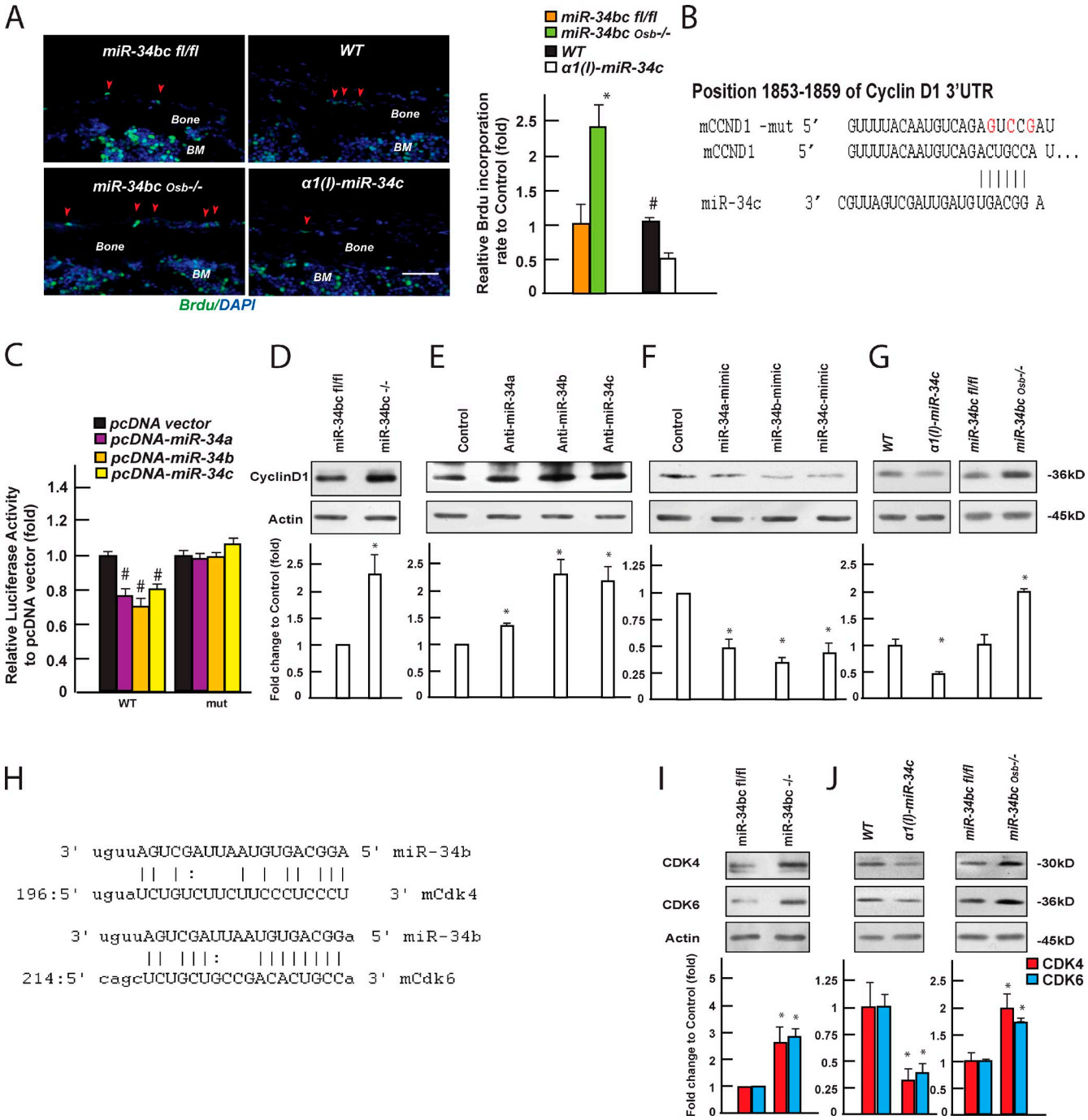

Figure 4. **miR-34b and -c regulate osteoblast proliferation.** (A) Proliferation of osteoblasts in miR-34bc$^{Osb-/-}$ and *α1(I)* miR-34c transgenic mice at p14, measured by BrdU incorporation (n = 3–5). Representative images of a BrdU incorporation assay in calvaria of miR-34bc$^{Osb-/-}$ mice and *α1(I)* miR-34c transgenic mice at p14. The first two layers of cells lining the cortical bone surface were typed as osteoblasts. Proliferating osteoblasts (arrowheads) were BrdU-positive cells (green), and nuclei were stained as blue (DAPI). BM, bone marrow. Bar, 20 µm. (B) Alignment of miR-34s showing complementary pairing to the 3′ UTRs of *Cyclin D1*. (C) Effect of miR-34 expression on luciferase reporter plasmids carrying either WT or mutant *Cyclin D1* 3′ UTRs (n = 3). #, $P < 0.001$. (D–G) Effect of knockdown (D and E) and overexpressing miR-34s (F) on Cyclin D1 protein level, as well as Cyclin D1 protein level in bones of miR-34bc$^{Osb-/-}$ and *α1(I)* miR-34c mice (G; n = 3–5 of each genotype), determined by Western blot and quantified using ImageJ. Quantification of Western blots was summarized from at least three independent experiments. (H) Alignment of miR-34s showing complementary pairing to the 3′ UTRs of *CDK4* and *CDK6*. (I) CDK4 and CDk6 protein levels in miR-34bc$^{-/-}$ osteoblasts. (J) CDK4 and CDk6 protein levels in bones of miR-34bc$^{Osb-/-}$ and *α1(I)* miR-34c mice (n = 3–5 of each genotype). Error bars indicate means ± standard errors of the mean. *, $P \leq 0.05$.

Likewise, there was premature ECM mineralization in digits of miR-34bc$^{Osb-/-}$ embryos (Fig. 5 D). Consistent with the alizarin red staining, histological analysis of tibia at E13.5 and E14.5 showed the presence of a mineralized bone collar at E13.5, and of nascent trabecula at E14.5 in miR-34bc$^{Osb-/-}$ mice, but not in control bones (Fig. 5 E). Quantitative real-time PCR revealed a significant increase in *Osteocalcin* expression at E14.5 and E16.5 miR-34bc$^{Osb-/-}$ calvaria (Fig. 5 F).

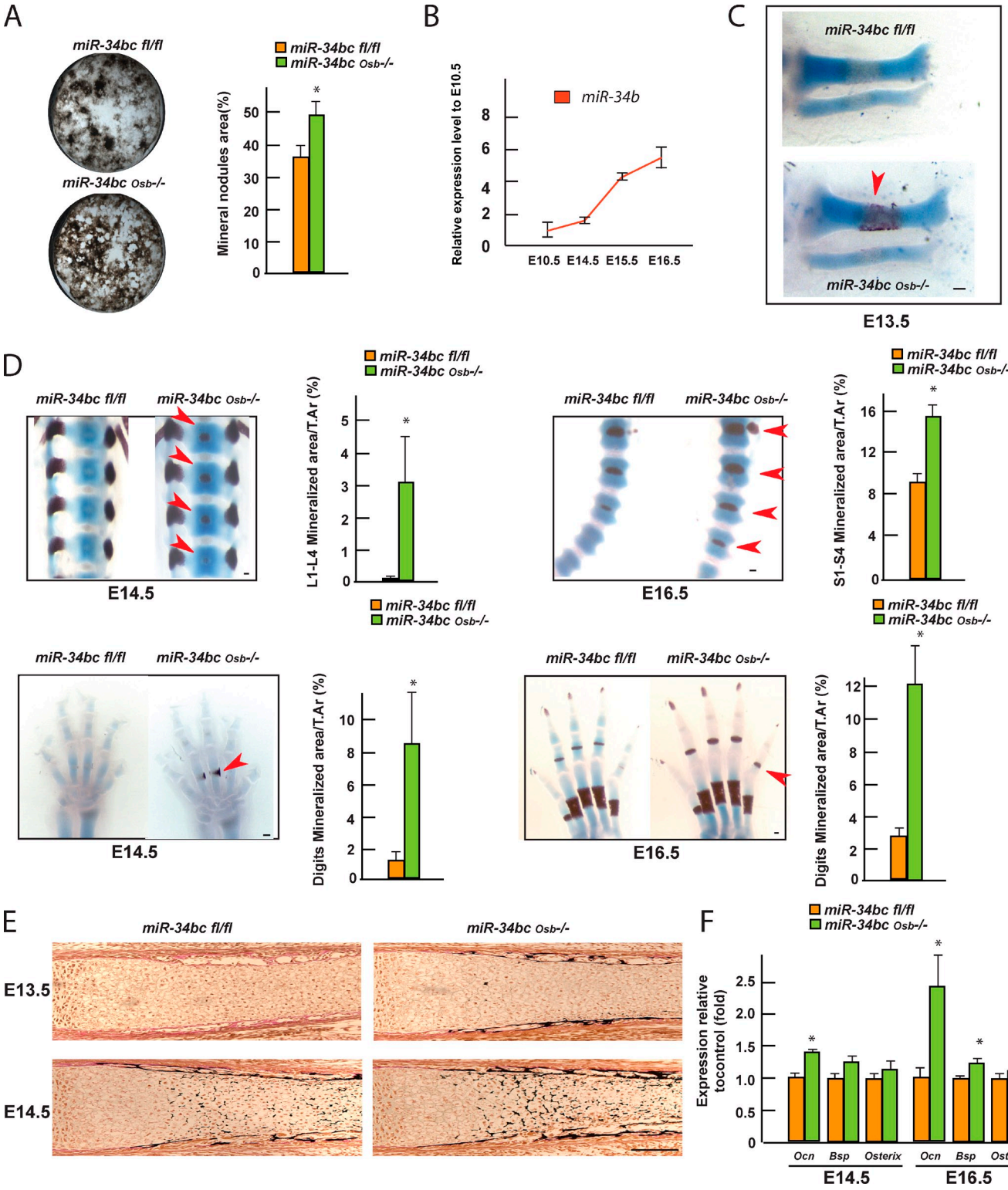

Figure 5. **miR-34b and -c regulate osteoblast differentiation.** (A) Mineralized nodule formation of control and miR-34bc$^{Osb-/-}$ osteoblasts after 2 wk of differentiation ex vivo, determined by Von Kossa staining and quantified by ImageJ (n = 3). (B) Expression of miR-34b in tibiae of E10.5, E14.5 E15.5, and E16.5 embryos. (C and D) Alcian blue/alizarin red staining of skeletal preparations of miR-34bc$^{Osb-/-}$ embryos. Arrowheads point to regions of premature ECM mineralization in miR-34bc$^{Osb-/-}$ embryos. The area of mineralization over tissue area was measured using ImageJ (E14.5, n = 6; E16.5, n = 3–4). (E) Representative images of Von Kossa/Von Geisen staining of tibia in E13.5 and E14.5 miR-34bc$^{Osb-/-}$ embryos. (F) Expression of *Osteocalcin*, *Bsp*, and *Osterix* in calvaria of E14.5 and E16.5 miR-34bc$^{Osb-/-}$ embryos (n = 3–5). Error bars indicate means ± standard errors of the mean. *, P ≤ 0.05. Bar, 100 µm.

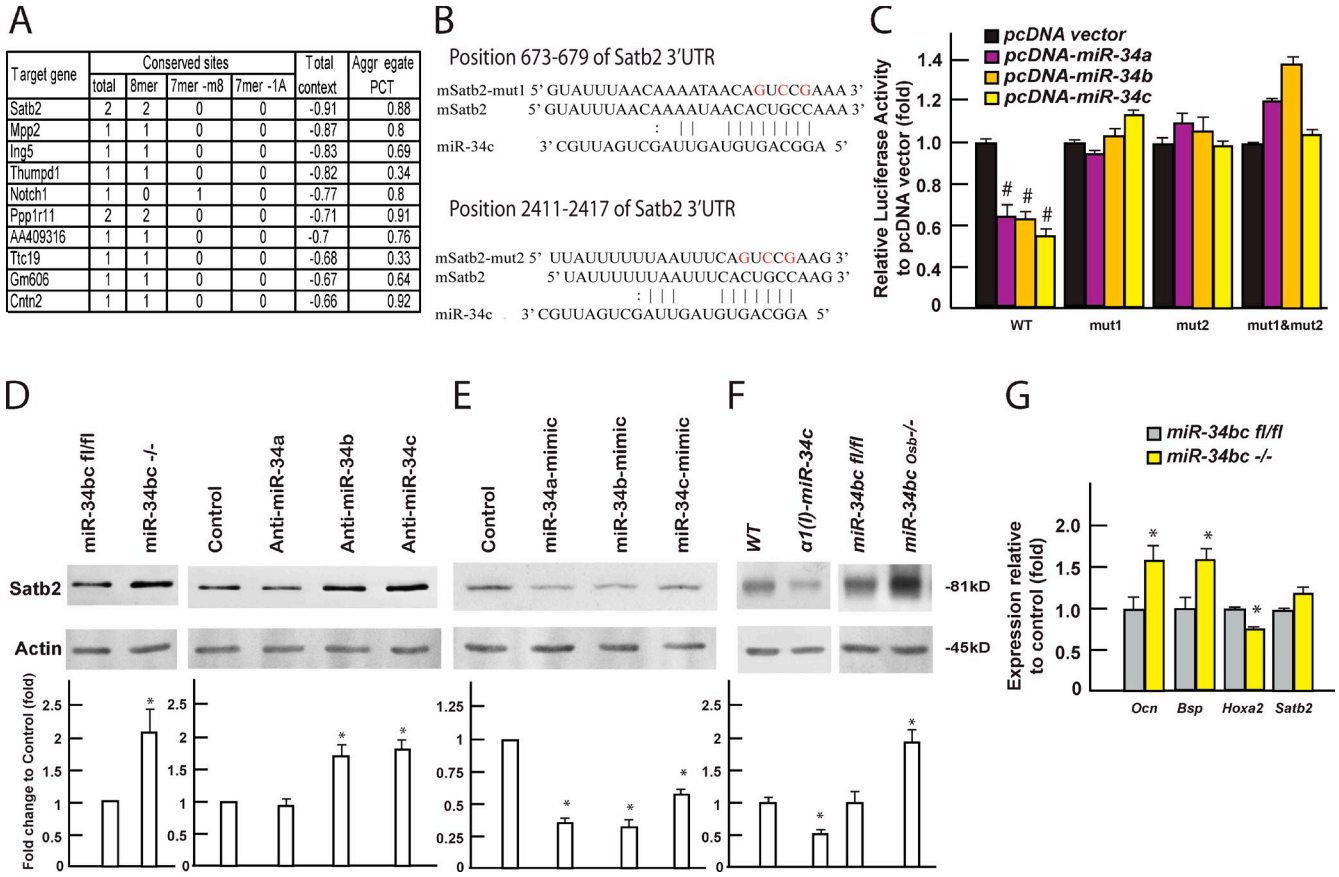

Target gene	Conserved sites				Total context	Aggr egate PCT
	total	8mer	7mer -m8	7mer -1A		
Satb2	2	2	0	0	-0.91	0.88
Mpp2	1	1	0	0	-0.87	0.8
Ing5	1	1	0	0	-0.83	0.69
Thumpd1	1	1	0	0	-0.82	0.34
Notch1	1	0	1	0	-0.77	0.8
Ppp1r11	2	2	0	0	-0.71	0.91
AA409316	1	1	0	0	-0.7	0.76
Ttc19	1	1	0	0	-0.68	0.33
Gm606	1	1	0	0	-0.67	0.64
Cntn2	1	1	0	0	-0.66	0.92

Figure 6. **miR-34b and -c regulate osteoblast differentiation by inhibiting Satb2 accumulation.** (A) List of top 10 putative targets of miR-34s identified by in silico analysis (TargetScanMouse5.2). (B) Alignment of miR-34c showing complementary pairing to the *Satb2* 3′ UTR. (C) Effect of miR-34 expression on luciferase reporter plasmids carrying either WT or mutant *Satb2* 3′ UTRs ($n = 3$). #, $P < 0.001$. (D and E) Effect of knockdown (D) and overexpressing miR-34s (E) on SATB2 protein level, determined by Western blotting and quantified using ImageJ. Quantification of Western blots was summarized from at least three independent experiments. (F) SATB2 protein level in bones of *α1(I)* miR-34c mice and miR-34bc$^{Osb-/-}$ (shown as the prominent upper band, $n = 3$–10 of each genotype). (G) mRNA level of osteoblast markers in miR-34bc$^{-/-}$ osteoblasts ($n = 3$). Error bars indicate means ± standard errors of the mean. *, $P \leq 0.05$.

A similar increase was seen in E16.5 miR-34bc$^{Osb-/-}$ calvaria for *Bsp* expression (Fig. 5 F). Consistent with the cell-specific nature of the gene deletion, there was no overt difference in the growth plate cartilage between miR-34bc$^{Osb-/-}$ and control embryos (Fig. S5 A). Collectively, these data indicate that miR-34b and -c regulate osteoblast differentiation during embryonic development.

Molecular basis of miR-34 regulation of osteoblast differentiation

To determine the molecular basis of the regulation of osteoblast differentiation by miR-34s, we again used in silico approaches (TargetScan and microRNA.org) to identify putative target genes of miR-34s whose relevance could be ascertained through loss-of-function experiments in the mouse. Two putative targets emerged from this survey.

The first hit in this list of 324 predicted target genes was *Satb2* (Fig. 6 A).

Several lines of evidence verified that *Satb2* is a bona fide target of miR-34s. First, sequence analysis revealed that there are two conserved binding sites for miR-34s in *Satb2* 3′ UTR: one at 673–679 and another one at 2,411–2,417 (Fig. 6 B). Second, in DNA cotransfection assays performed in COS cells, forced expression of either member of the miR-34 family inhibited luciferase activity of a vector containing the WT 3′ UTR of *Satb2*, but not a mutated *Satb2* 3′ UTR in which either one or both miR-34 binding sites had been mutated (Fig. 6 C). Third, in miR-34bc$^{-/-}$ osteoblasts and in primary osteoblasts transfected with specific inhibitors of miR-34b and -c, or, to a lower extent, of miR-34a, Western blot analysis showed an increase in SATB2 protein (Fig. 6 D). Conversely, forced expression of each member of the miR-34 family in osteoblasts resulted in a 50–70% decrease in SATB2 protein (Fig. 6 E), whereas deletion of miR-34s did not affect the *Satb2* mRNA level (Fig. 6 G). Fourth, and in a mirror image of what is seen in *Satb2*$^{-/-}$ osteoblasts (Dobreva et al., 2006), *Ocn* and *Bsp* expression was increased while *Hoxa2* expression was decreased in miR-34bc$^{-/-}$ osteoblasts (Fig. 6 G). Lastly, SATB2 protein levels were increased in bones of miR-34bc$^{Osb-/-}$ mice and decreased in bones of *α1(I)* miR-34c mice (Fig. 6 F).

We reasoned that if *Satb2* is a biologically relevant target of miR-34s, removing one allele of this gene from miR-34bc$^{Osb-/-}$ mice should correct their phenotypic and molecular abnormalities. Indeed, we observed that removing one allele of *Satb2* from miR-34bc$^{Osb-/-}$ mice normalized its protein level in bones

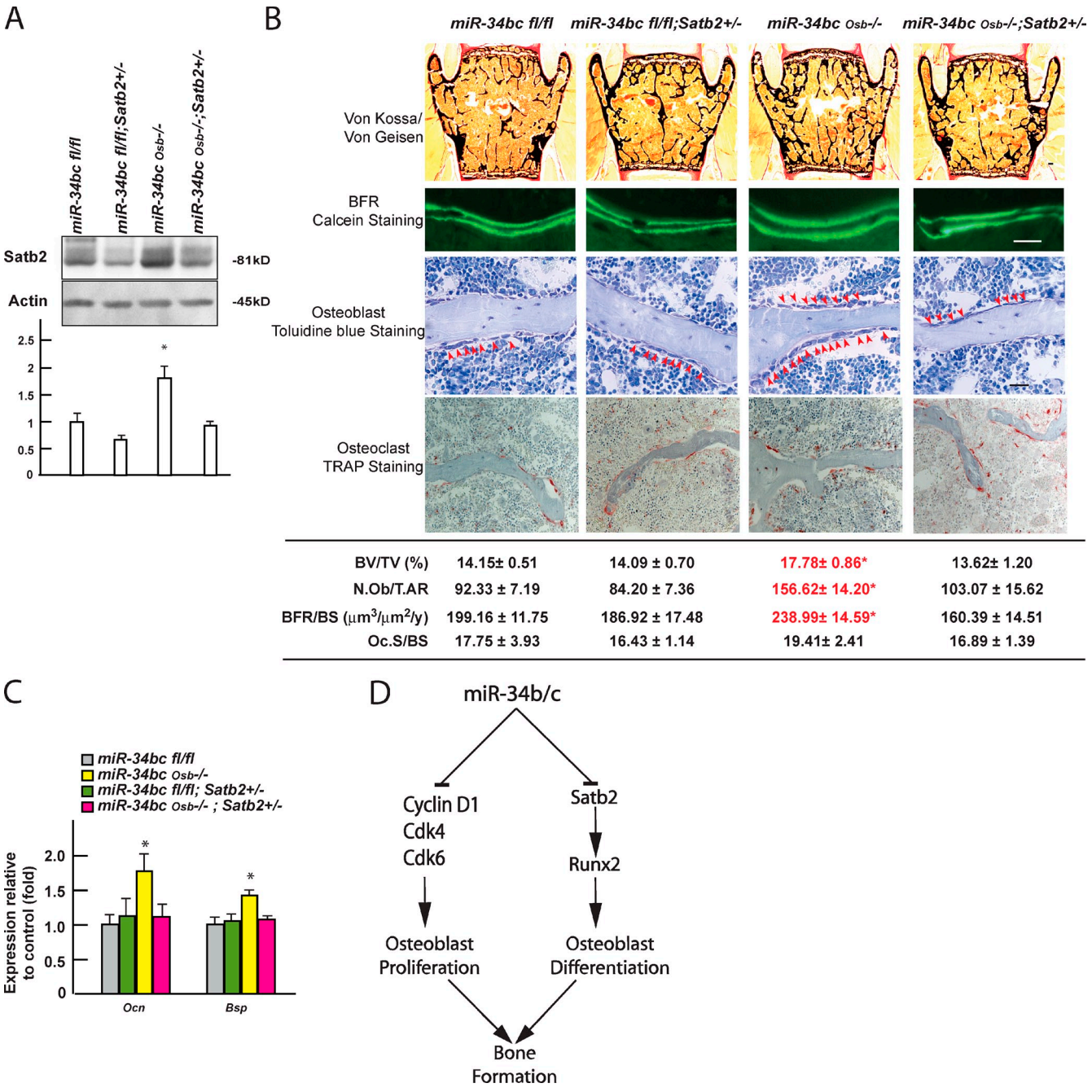

	miR-34bc fl/fl	miR-34bc fl/fl;Satb2+/-	miR-34bc Osb-/-	miR-34bc Osb-/-;Satb2+/-
BV/TV (%)	14.15± 0.51	14.09 ± 0.70	17.78± 0.86*	13.62± 1.20
N.Ob/T.AR	92.33 ± 7.19	84.20 ± 7.36	156.62± 14.20*	103.07 ± 15.62
BFR/BS ($\mu m^3/\mu m^2/y$)	199.16 ± 11.75	186.92 ± 17.48	238.99± 14.59*	160.39 ± 14.51
Oc.S/BS	17.75 ± 3.93	16.43 ± 1.14	19.41± 2.41	16.89 ± 1.39

Figure 7. **miR-34b and -c regulate bone mass accrual in a Satb2-dependent manner.** (A) SATB2 protein level in bones of miR-34bc$^{Osb-/-}$;Satb2$^{+/-}$ mice (n = 3–10 of each genotype). (B) Histomorphometric analysis of L3 and L4 vertebrae of miR-34bc$^{Osb-/-}$;Satb2$^{+/-}$ mice (n = 7–12) at 3 mo of age. Representative histological images were shown. Bar, 20 µm. (C) Expression level of *Osteocalcin* and *Bsp* in bones of miR-34bc$^{Osb-/-}$;Satb2$^{+/-}$ mice (n = 5–9), determined by qPCR. Asterisks in A, B, and C indicate that miR-34bc$^{Osb-/-}$ mice are significantly different from the other groups; $P \leq 0.05$. Error bars indicate means ± standard errors of the mean. (D) Model of the functions of miR-34s in osteoblasts.

(Fig. 7 A), but also normalized bone mass, BFR, and the number of osteoblasts in miR-34bc$^{Osb-/-}$ mice (Fig. 7 B). Likewise, expression of *Osteocalcin* and *Bsp* was similar in miR-34bc$^{fl/fl}$ and miR-34bc$^{Osb-/-}$;Satb2$^{+/-}$ mice, and lower than in miR-34bc$^{Osb-/-}$ mice at 3 mo of age (Fig. 7 C). These data provide an in vivo verification of the importance of SATB2 regulation by miR-34b and -c in osteoblasts in vivo.

The fifth hit in this list was *Notch1*, an important determinant of skeletogenesis (Engin et al., 2008; Hilton et al., 2008) that is also a regulator of *Cyclin D1* expression (Ronchini and Capobianco, 2001). Hence, we asked whether Notch1 accumulation was affected by miR-34b/c deletion and if it was the cause of the decreased levels of Cyclin D1 observed in miR-34bc$^{Osb-/-}$ bones. However, Cyclin D1 accumulation was increased in miR-34bc$^{-/-}$ osteoblasts, whereas Notch1 was not (Fig. S5 B). This experiment indicates that miR-34b and -c regulates Cyclin D1 accumulation in a Notch1-independent manner.

Discussion

The cell-specific loss-of-function experiments presented here provide in vivo evidence that miRNAs play a role in osteoblast proliferation and differentiation occurring during embryogenesis and postnatally, and identify miR-34b and -c as two such miRNAs. To the best of our knowledge these are the first miRNAs shown to affect osteoblast differentiation and proliferation in vivo through identifiable pathways (Fig. 7 D).

A remarkable feature of these two miRNAs is that their influence on osteoblast biology is observed in unchallenged mice. This observation contrasts with the fact that the functions of many miRNAs involved in the development of the heart, an organ where they have been intensively studied, are revealed only in challenged animals (van Rooij et al., 2009; Williams et al., 2009; Liu and Olson, 2010; Small et al., 2010). This observation, together with the dual pre- and postnatal role of miR-34s, underscores their importance in bone development and physiology. Importantly, our initial screen suggests that other miRNAs may influence skeletogenesis and bone mass accrual as well. Therefore, our results are an incentive to determine if and how they may affect bone formation in unchallenged mice.

Our in vivo analysis showed that miR-34b/c affects osteoblast proliferation without affecting osteoclast number and bone resorption. This observation, together with the analyses of other animal models in which bone formation and bone resorption are not coordinately regulated (Corral et al., 1998; Elefteriou et al., 2005), provide further evidence that bone formation and bone resorption need not be coupled in vivo (Ducy et al., 2000). The fact that miR-34s affect osteoblast proliferation and bone formation so significantly without affecting bone resorption raises the prospect that they may also be implicated in the recently uncovered regulation of bone formation by gut-derived serotonin (Yadav et al., 2008).

To elucidate the molecular basis underlying miR-34 regulation of bone, we used in silico analyses and identified *Cyclin D1*, *Cdk4*, and *Cdk6* as potential targets for these miRNAs (He et al., 2007; Lee et al., 2011). Further analysis of the *CyclinD1*, *Cdk4*, and *Cdk6* 3′ UTR identified bona fide miR-34 binding sites (Fig. 4 B and H), and Western blots of miR-34bc$^{-/-}$ osteoblasts verified that accumulation of these three proteins was regulated by miR-34s in osteoblasts. However, it is likely that other genes affecting cell cycle progression may be targets of miR-34b and -c in osteoblasts as well. A more systematic analysis of all the putative targets of these two miRNAs will allow us to address this question.

In addition to osteoblast proliferation, miR-34b and -c influence rather profoundly the differentiation of mesenchymal cell progenitors along the osteoblast lineage. Analysis of this function of miR-34s allowed us to uncover these mechanisms of action in vivo. Indeed, among many candidate targets that could mediate their function, the first one to emerge was SATB2. Molecular and genetic evidence showed that it is a target of miR-34b and -c, and is most likely the main molecular mechanism responsible for miR-34 regulation of osteoblast differentiation, at least during the postnatal period. The direct regulation of SATB2 by miR-34s explains why these miRNAs regulate *Osteocalcin*, *Bsp*, and possibly other genes whose expression is controlled by Runx2 and SATB2 or ATF4 and SATB2. Because the osteoblast differentiation defect in miR-34bc$^{Osb-/-}$ mice is initiated during embryonic development, it will be interested to study whether SATB2 is also the main target of miR-34s in developing osteoblasts during skeletogenesis. However, we remain fully aware that *Sabt2* may not be the only target of miR-34s in regulation of osteoblast differentiation, and our result does not exclude the possibility that other putative targets, such as *Notch1* and/or other genes yet to be identified, may additionally account for the ability of miR-34b and -c to regulate osteoblast differentiation during development.

In summary, this work illustrates the emerging importance of this mode of regulation for organogenesis by expanding it to the skeleton. Moreover, using genetic approaches to identify the nuclear matrix protein Satb2 as a target of miR-34s provides one molecular mechanism whereby miR-34s modulate osteoblast differentiation in vivo.

Materials and methods

Mice generation

To generate osteoblast-specific miR-34s–deficient mice, targeting vectors harboring LoxP sites, as well as a flippase recognition target (FRT)-framed neomycin resistance cassette, were electroporated into embryonic stem (ES) cells (CSL3,129/SvEvTac; Columbia Presbyterian Cancer Center Transgenic Facility; Fig. S3, A and B). ES cells containing the floxed allele were injected in 129Sv/EV blastocysts to generate chimeric mice. Chimeric mice were crossed to Gt(ROSA)26Sor$^{tm1(FLP1)Dym}$ mice (10 times backcrossed to C57/B6, obtained from The Jackson Laboratory) to remove the neomycin resistance cassette and to generate *flox/+* mice. *Flox/+* mice were then crossed with *α1(I)Col-Cre* mice (10 times backcrossed to C57/B6) to generate *Osb*$^{+/-}$ mice, whose progenies were intercrossed to obtain *Osb*$^{-/-}$ mice. miR-34abc$^{Osb-/-}$ mice were obtained by intercrossing miR-34a$^{Osb-/-}$ *and* miR-34bc$^{Osb-/-}$ mice. To generate *α1(I)* miR-34c transgenic mice, a cDNA fragment of the miR-34c was cloned into a plasmid containing a 2.3-kb *α1(I)* collagen promoter and microinjected using standard protocols. *Satb2*$^{+/-}$ mice were generated previously by inserting a β-galactosidase/pGKneo-pA cassette in frame with the ATG codon of the SATB2 gene (Dobreva et al., 2006). Except for *α1(I)* miR-34c transgenic, which had been backcrossed five times with C57/B6, all other mice analyzed were maintained on a C57/129 mixed background.

Cell culture and transfection

Primary mouse calvaria osteoblasts were cultured as described previously (Ducy and Karsenty, 1995). In brief, osteoblasts from calvaria of newborn pups were isolated by sequential digestion of 15, 30, and 45 min in αMEM medium containing 0.1 mg/ml collagenase P-10% trypsin, and were cultured in αMEM/10% FBS for 2 d. Thereafter, to induce osteoblast differentiation, the medium was supplemented with 5 mM β-glycerophosphate and 100 µg/ml ascorbic acid, and replaced every 2 d. miR-34bc$^{-/-}$ calvaria osteoblasts were generated ex vivo by infecting miR-34bc$^{fl/fl}$ osteoblasts with either GFP- or Cre-GFP–expressing adenovirus (University of Iowa). miRIDIAN mimics and hairpin inhibitors of miR-34s were purchased from Thermo Fisher Scientific, Inc., and transfected using DharmaFECT transfection reagents as described by the manufacturer (Thermo Fisher Scientific). 48 h after transfection, protein samples were extracted for Western blots.

Microarray and qPCR

Microarray analysis was performed using the miRCURY LNA microRNA Array system (Exiqon). For detection of miRNA, RNA purification was performed using miRNeasy Mini kit (QIAGEN), and cDNA synthesis and qPCR were performed according to the TaqMan Small RNA assay's instructions (Applied Biosystems). Relative expression levels of each miRNA were normalized to *U6* expression levels. For quantifying gene expression, unless specified in the figure legend, femurs and tibiae of 3-mo-old

mice were used for RNA preparation. After femurs and tibiae were dissected out, connective tissue and growth plate were removed and bone marrow cells were flushed out with 1× PBS before isolating RNA. Bone RNA samples were purified using TRIZOL reagent (Invitrogen). 2 µg of total RNA was reverse transcribed into cDNA using M-MLV reverse transcription (Invitrogen) in a 50-µl reaction volume, then 1.5 µl of cDNA was used for qPCR. Relative expression levels of each gene were normalized to 18S ribosomal RNA levels.

Luciferase reporter assay
A pMIR-REPORT miRNA Expression Reporter Vector system was used for luciferase reporter assays and performed according to manufacturer's instructions (Invitrogen). WT or mutated 3′ UTRs of *Satb2* and *Cyclin D1* were subcloned downstream of the luciferase gene in the pMIR-REPORT luciferase vector, and cDNAs of miR-34s were cloned into the pcDNA3.0 vector. These vectors were then cotransfected into COS-7 cells along with pMIR-REPORT β-gal control plasmid. After 24 h, luciferase activity was measured and normalized to β-galactosidase levels as described previously (Ducy and Karsenty, 1995). In brief, cells were harvested and lysed in 0.25 M Tris-HCl, pH 7.9, by three cycles of freeze-thawing. Luciferase activities were assayed by using D-luciferin substrate (Sigma-Aldrich) in 100 mM potassium phosphate, pH 7.8, 5 mM ATP, 15 mM $MgSO_4$, and 1 mM dithiothreitol, and measured in a Monolight 2010 luminometer (Analytical Luminescence Laboratory). β-Galactosidase activities present in each lysate were measured by a colorimetric enzyme assay using resorufin β-D-galactopyranoside (Sigma-Aldrich) as a substrate. Relative luciferase activity was calculated with respect to cells transfected with pcDNA3.0 vector.

In silico analysis
In silico analysis of putative targets of miRNA were performed using two databases: TargetScanMouse5.2 (http://www.targetscan.org/mmu_50/) and microRNA.org, Targets and Expression. The putative targets were ranked according to the total context score value of the conserved sites (the lower value; i.e., the more favorable target).

Northern and Western blot analyses
Northern and Western blot analyses were performed according to standard protocols. Antibodies used were anti-SATB2, Notch1, Cyclin E2, E2F3, E2F5 (Abcam), anti–Cyclin D1, β-Actin, CDK4, CDK6, and MET (Cell Signaling Technology). Quantification of Western blots was performed using ImageJ. Protein levels were quantified and normalized to β-Actin levels. Relative protein levels were calculated with respect to control samples.

Serum biochemistry
ELISA was used to measure serum Osteocalcin (Biomedical Technologies, Inc.) and Ctx (RatLaps; IDS), and performed according to manufacturer's instructions.

Proliferation and cell death assay
BrdU was IP injected in P14 mice at a dose of 100 µg/g 16 h before sacrifice. Calvaria bones were dissected and fixed in 4% PFA overnight. These samples were decalcified in 14% EDTA for 3 d, soaked in 30% sucrose in PBS for 1 d, embedded in OCT compound (Tissue-Tek), and sectioned at 5 µm. BrdU incorporation was detected by using a commercial BrdU detection kit (Roche). A TUNEL assay was performed using an In Situ Cell Death Detection kit (Roche).

Skeleton preparation, histology, and histomorphometry
Skeleton preparations and alcian blue/alizarin red staining were performed according to standard protocols (McLeod, 1980). In brief, mouse skeletons at each indicated time point of development were dissected and fixed in 95% ethanol at 4°C overnight, and stained with 0.015% Alcian blue 8GX dye (Sigma-Aldrich) for 1 d, followed by staining with 0.005% Alizarin red solution (Sigma-Aldrich) overnight. Specimens were cleared and stored in 50% glycerol/50% ethanol.

Bone histology and histomorphometry were performed at the site of L3 and L4 vertebrae in 3-mo-old female mice, as described previously (Chappard et al., 1987; Parfitt et al., 1987). In brief, vertebrae were dissected out and fixed in 4% formaldehyde for 18 h at 4°C. Undecalcified bones were embedded in methyl methacrylate, and 5–7-µm sections were prepared on a rotation microtome. For mineralized bone volume over the total tissue volume (BV/TV), sections were stained with von Kossa reagent (3% silver nitrate) counterstained with Van Gieson solution (Sigma-Aldrich). BFR (the annual fractional volume of trabecular bone formed per unit trabecular surface area, BFR/BS) was analyzed by the calcein double-labeling method. Accordingly, mice were injected twice with 20 mg/kg calcein 7 and 2 d, respectively, before sacrifice. For the analysis of parameters of osteoblasts (osteoblast number per tissue area, N.Ob/T.Ar), bone sections were stained with 1% toluidine blue. For the analysis of parameters of osteoclasts (osteoclast surface per bone surface, Oc.S/BS), bone sections were incubated for 30 min in TRAP staining solution at 37°C and then counterstained with hematoxylin. Osteoclasts were defined as multinucleated dark red cells along the bone surface. Histological sections were viewed under a microscope (DMLB; Leica) using a 40× objective lens at RT. Histomorphometric analysis was performed using the Osteomeasure System (OsteoMetrics).

µCT analysis
Cortical bone architecture of femur was assessed using a µCT system (VivaCT 40; SCANCO Medical AG). Cortical bone volume, mineralization density, and midshaft thickness were analyzed using the standard software provided by the manufacturer of the µCT scanner.

Statistics
All data are presented as means ± standard errors of the mean. Statistical analyses were performed using unpaired, two-tailed Student's *t* tests. For all experiments, *, $P \leq 0.05$; #, $P \leq 0.001$.

Microscopy
Histological stained embryos and osteoblast cultures were viewed under a dissecting microscope (MZ95; Leica) using a 1× objective lens at RT. Histological sections of Von Kossa/Van Gieson staining were viewed under a light microscope (4000B; Leica) using 5× (adults) or 10× (embryos) objective lenses at RT. BrdU and TUNEL staining were viewed under a fluorescent microscope (4000B; Leica) using a 20× objective lens at RT. All images were acquired with a camera (DFC300FX; Leica) and FireCam image software (Leica). Images were processed with Photoshop (Adobe), and imaged figures were constructed in Illustrator (Adobe).

Online supplemental material
Fig. S1 provides tissue expression pattern of miR-34b and -c in WT mice comparing to miR-22, -146b, -24–2, -23a, and -27a. Fig. S2 provides serum Ctx level of *α1(I)* miR-34c transgenic mice. Fig. S3 provides targeting strategy of miR-34a$^{Osb-/-}$ mice and miR-34bc$^{Osb-/-}$ mice, and recombination efficiency of miR-34s in these mutant mice. Fig. S4 provides the quantification data of a TUNEL assay of *α1(I)* miR-34c transgenic and miR-34bc$^{Osb-/-}$ mice. Fig. S5 shows the growth plate of femur in E14.5 miR-34bc$^{fl/fl}$ and miR-34bc$^{Osb-/-}$ embryos. Online supplemental material is available at http://www.jcb.org/cgi/content/full/jcb.201201057/DC1.

The authors thank C. Liu for technical assistance and Drs. P. Ducy, S. Kousteni, and R. Wagner for critical reading of the manuscript.

This work was supported by National Institutes of Health grant R01DK067936 (to G. Karsenty). The work of H. Inose was supported in part by Grants-in-Aid for Scientific Research.

Submitted: 11 January 2012
Accepted: 5 April 2012

References

Bakker, A., and J. Klein-Nulend. 2003. Osteoblast isolation from murine calvariae and long bones. *Methods Mol. Med.* 80:19–28.

Bartel, D.P. 2009. MicroRNAs: target recognition and regulatory functions. *Cell.* 136:215–233. http://dx.doi.org/10.1016/j.cell.2009.01.002

Bialek, P., B. Kern, X. Yang, M. Schrock, D. Sosic, N. Hong, H. Wu, K. Yu, D.M. Ornitz, E.N. Olson, et al. 2004. A twist code determines the onset of osteoblast differentiation. *Dev. Cell.* 6:423–435. http://dx.doi.org/10.1016/S1534-5807(04)00058-9

Bozec, A., L. Bakiri, M. Jimenez, T. Schinke, M. Amling, and E.F. Wagner. 2010. Fra-2/AP-1 controls bone formation by regulating osteoblast differentiation and collagen production. *J. Cell Biol.* 190:1093–1106. http://dx.doi.org/10.1083/jcb.201002111

Chappard, D., S. Palle, C. Alexandre, L. Vico, and G. Riffat. 1987. Bone embedding in pure methyl methacrylate at low temperature preserves enzyme activities. *Acta Histochem.* 81:183–190. http://dx.doi.org/10.1016/S0065-1281(87)80012-0

Corral, D.A., M. Amling, M. Priemel, E. Loyer, S. Fuchs, P. Ducy, R. Baron, and G. Karsenty. 1998. Dissociation between bone resorption and bone

formation in osteopenic transgenic mice. *Proc. Natl. Acad. Sci. USA*. 95:13835–13840. http://dx.doi.org/10.1073/pnas.95.23.13835

Dacquin, R., M. Starbuck, T. Schinke, and G. Karsenty. 2002. Mouse alpha1(I)-collagen promoter is the best known promoter to drive efficient Cre recombinase expression in osteoblast. *Dev. Dyn.* 224:245–251. http://dx.doi.org/10.1002/dvdy.10100

Djuranovic, S., A. Nahvi, and R. Green. 2011. A parsimonious model for gene regulation by miRNAs. *Science*. 331:550–553. http://dx.doi.org/10.1126/science.1191138

Dobreva, G., M. Chahrour, M. Dautzenberg, L. Chirivella, B. Kanzler, I. Fariñas, G. Karsenty, and R. Grosschedl. 2006. SATB2 is a multifunctional determinant of craniofacial patterning and osteoblast differentiation. *Cell*. 125:971–986. http://dx.doi.org/10.1016/j.cell.2006.05.012

Ducy, P., and G. Karsenty. 1995. Two distinct osteoblast-specific cis-acting elements control expression of a mouse osteocalcin gene. *Mol. Cell. Biol.* 15:1858–1869.

Ducy, P., R. Zhang, V. Geoffroy, A.L. Ridall, and G. Karsenty. 1997. Osf2/Cbfa1: a transcriptional activator of osteoblast differentiation. *Cell*. 89:747–754. http://dx.doi.org/10.1016/S0092-8674(00)80257-3

Ducy, P., T. Schinke, and G. Karsenty. 2000. The osteoblast: a sophisticated fibroblast under central surveillance. *Science*. 289:1501–1504. http://dx.doi.org/10.1126/science.289.5484.1501

Elefteriou, F., J.D. Ahn, S. Takeda, M. Starbuck, X. Yang, X. Liu, H. Kondo, W.G. Richards, T.W. Bannon, M. Noda, et al. 2005. Leptin regulation of bone resorption by the sympathetic nervous system and CART. *Nature*. 434:514–520. http://dx.doi.org/10.1038/nature03398

Engin, F., Z. Yao, T. Yang, G. Zhou, T. Bertin, M.M. Jiang, Y. Chen, L. Wang, H. Zheng, R.E. Sutton, et al. 2008. Dimorphic effects of Notch signaling in bone homeostasis. *Nat. Med.* 14:299–305. http://dx.doi.org/10.1038/nm1712

Eyre, D.R., I.R. Dickson, and K. Van Ness. 1988. Collagen cross-linking in human bone and articular cartilage. Age-related changes in the content of mature hydroxypyridinium residues. *Biochem. J.* 252:495–500.

Gaur, T., S. Hussain, R. Mudhasani, I. Parulkar, J.L. Colby, D. Frederick, B.E. Kream, A.J. van Wijnen, J.L. Stein, G.S. Stein, et al. 2010. Dicer inactivation in osteoprogenitor cells compromises fetal survival and bone formation, while excision in differentiated osteoblasts increases bone mass in the adult mouse. *Dev. Biol.* 340:10–21. http://dx.doi.org/10.1016/j.ydbio.2010.01.008

Glass, D.A. II, P. Bialek, J.D. Ahn, M. Starbuck, M.S. Patel, H. Clevers, M.M. Taketo, F. Long, A.P. McMahon, R.A. Lang, and G. Karsenty. 2005. Canonical Wnt signaling in differentiated osteoblasts controls osteoclast differentiation. *Dev. Cell*. 8:751–764. http://dx.doi.org/10.1016/j.devcel.2005.02.017

Hassan, M.Q., J.A. Gordon, M.M. Beloti, C.M. Croce, A.J. van Wijnen, J.L. Stein, G.S. Stein, and J.B. Lian. 2010. A network connecting Runx2, SATB2, and the miR-23a~27a~24-2 cluster regulates the osteoblast differentiation program. *Proc. Natl. Acad. Sci. USA*. 107:19879–19884. http://dx.doi.org/10.1073/pnas.1007698107

He, L., X. He, L.P. Lim, E. de Stanchina, Z. Xuan, Y. Liang, W. Xue, L. Zender, J. Magnus, D. Ridzon, et al. 2007. A microRNA component of the p53 tumour suppressor network. *Nature*. 447:1130–1134. http://dx.doi.org/10.1038/nature05939

Hilton, M.J., X. Tu, X. Wu, S. Bai, H. Zhao, T. Kobayashi, H.M. Kronenberg, S.L. Teitelbaum, F.P. Ross, R. Kopan, and F. Long. 2008. Notch signaling maintains bone marrow mesenchymal progenitors by suppressing osteoblast differentiation. *Nat. Med.* 14:306–314. http://dx.doi.org/10.1038/nm1716

Huntzinger, E., and E. Izaurralde. 2011. Gene silencing by microRNAs: contributions of translational repression and mRNA decay. *Nat. Rev. Genet.* 12:99–110. http://dx.doi.org/10.1038/nrg2936

Johnnidis, J.B., M.H. Harris, R.T. Wheeler, S. Stehling-Sun, M.H. Lam, O. Kirak, T.R. Brummelkamp, M.D. Fleming, and F.D. Camargo. 2008. Regulation of progenitor cell proliferation and granulocyte function by microRNA-223. *Nature*. 451:1125–1129. http://dx.doi.org/10.1038/nature06607

Jones, D.C., M.N. Wein, M. Oukka, J.G. Hofstaetter, M.J. Glimcher, and L.H. Glimcher. 2006. Regulation of adult bone mass by the zinc finger adapter protein Schnurri-3. *Science*. 312:1223–1227. http://dx.doi.org/10.1126/science.1126313

Kajimura, D., E. Hinoi, M. Ferron, A. Kode, K.J. Riley, B. Zhou, X.E. Guo, and G. Karsenty. 2011. Genetic determination of the cellular basis of the sympathetic regulation of bone mass accrual. *J. Exp. Med.* 208:841–851. http://dx.doi.org/10.1084/jem.20102608

Kanzler, B., S.J. Kuschert, Y.H. Liu, and M. Mallo. 1998. Hoxa-2 restricts the chondrogenic domain and inhibits bone formation during development of the branchial area. *Development*. 125:2587–2597.

Kenner, L., A. Hoebertz, F.T. Beil, N. Keon, F. Karreth, R. Eferl, H. Scheuch, A. Szremska, M. Amling, M. Schorpp-Kistner, et al. 2004. Mice lacking JunB are osteopenic due to cell-autonomous osteoblast and osteoclast defects. *J. Cell Biol.* 164:613–623. (published erratum appears in *J. Cell Biol*. 2011. 195:1063) http://dx.doi.org/10.1083/jcb.200308155

Kim, S., T. Koga, M. Isobe, B.E. Kern, T. Yokochi, Y.E. Chin, G. Karsenty, T. Taniguchi, and H. Takayanagi. 2003. Stat1 functions as a cytoplasmic attenuator of Runx2 in the transcriptional program of osteoblast differentiation. *Genes Dev*. 17:1979–1991. http://dx.doi.org/10.1101/gad.1119303

Kim, N.H., H.S. Kim, N.G. Kim, I. Lee, H.S. Choi, X.Y. Li, S.E. Kang, S.Y. Cha, J.K. Ryu, J.M. Na, et al. 2011. p53 and microRNA-34 are suppressors of canonical Wnt signaling. *Sci. Signal.* 4:ra71. http://dx.doi.org/10.1126/scisignal.2001744

Komori, T., H. Yagi, S. Nomura, A. Yamaguchi, K. Sasaki, K. Deguchi, Y. Shimizu, R.T. Bronson, Y.H. Gao, M. Inada, et al. 1997. Targeted disruption of Cbfa1 results in a complete lack of bone formation owing to maturational arrest of osteoblasts. *Cell*. 89:755–764. http://dx.doi.org/10.1016/S0092-8674(00)80258-5

Landgraf, P., M. Rusu, R. Sheridan, A. Sewer, N. Iovino, A. Aravin, S. Pfeffer, A. Rice, A.O. Kamphorst, M. Landthaler, et al. 2007. A mammalian microRNA expression atlas based on small RNA library sequencing. *Cell*. 129:1401–1414. http://dx.doi.org/10.1016/j.cell.2007.04.040

Lee, Y.M., J.Y. Lee, C.C. Ho, Q.S. Hong, S.L. Yu, C.R. Tzeng, P.C. Yang, and H.W. Chen. 2011. miRNA-34b as a tumor suppressor in estrogen-dependent growth of breast cancer cells. *Breast Cancer Res.* 13:R116. http://dx.doi.org/10.1186/bcr3059

Liu, N., and E.N. Olson. 2010. MicroRNA regulatory networks in cardiovascular development. *Dev. Cell*. 18:510–525. http://dx.doi.org/10.1016/j.devcel.2010.03.010

McLeod, M.J. 1980. Differential staining of cartilage and bone in whole mouse fetuses by alcian blue and alizarin red S. *Teratology*. 22:299–301. http://dx.doi.org/10.1002/tera.1420220306

Nakashima, K., X. Zhou, G. Kunkel, Z. Zhang, J.M. Deng, R.R. Behringer, and B. de Crombrugghe. 2002. The novel zinc finger-containing transcription factor osterix is required for osteoblast differentiation and bone formation. *Cell*. 108:17–29. http://dx.doi.org/10.1016/S0092-8674(01)00622-5

Parfitt, A.M., M.K. Drezner, F.H. Glorieux, J.A. Kanis, H. Malluche, P.J. Meunier, S.M. Ott, and R.R. Recker. 1987. Bone histomorphometry: standardization of nomenclature, symbols, and units. *J. Bone Miner. Res.* 2:595–610. http://dx.doi.org/10.1002/jbmr.5650020617

Poy, M.N., L. Eliasson, J. Krutzfeldt, S. Kuwajima, X. Ma, P.E. Macdonald, S. Pfeffer, T. Tuschl, N. Rajewsky, P. Rorsman, and M. Stoffel. 2004. A pancreatic islet-specific microRNA regulates insulin secretion. *Nature*. 432:226–230. http://dx.doi.org/10.1038/nature03076

Price, P.A., J.G. Parthemore, and L.J. Deftos. 1980. New biochemical marker for bone metabolism. Measurement by radioimmunoassay of bone GLA protein in the plasma of normal subjects and patients with bone disease. *J. Clin. Invest.* 66:878–883. http://dx.doi.org/10.1172/JCI109954

Rached, M.T., A. Kode, B.C. Silva, D.Y. Jung, S. Gray, H. Ong, J.H. Paik, R.A. DePinho, J.K. Kim, G. Karsenty, and S. Kousteni. 2010. FoxO1 expression in osteoblasts regulates glucose homeostasis through regulation of osteocalcin in mice. *J. Clin. Invest.* 120:357–368. http://dx.doi.org/10.1172/JCI39901

Ronchini, C., and A.J. Capobianco. 2001. Induction of cyclin D1 transcription and CDK2 activity by Notch(ic): implication for cell cycle disruption in transformation by Notch(ic). *Mol. Cell. Biol.* 21:5925–5934. http://dx.doi.org/10.1128/MCB.21.17.5925-5934.2001

Small, E.M., R.J. Frost, and E.N. Olson. 2010. MicroRNAs add a new dimension to cardiovascular disease. *Circulation*. 121:1022–1032. http://dx.doi.org/10.1161/CIRCULATIONAHA.109.889048

Valencia-Sanchez, M.A., J. Liu, G.J. Hannon, and R. Parker. 2006. Control of translation and mRNA degradation by miRNAs and siRNAs. *Genes Dev.* 20:515–524. http://dx.doi.org/10.1101/gad.1399806

van Rooij, E., D. Quiat, B.A. Johnson, L.B. Sutherland, X. Qi, J.A. Richardson, R.J. Kelm Jr., and E.N. Olson. 2009. A family of microRNAs encoded by myosin genes governs myosin expression and muscle performance. *Dev. Cell*. 17:662–673. http://dx.doi.org/10.1016/j.devcel.2009.10.013

Williams, A.H., G. Valdez, V. Moresi, X. Qi, J. McAnally, J.L. Elliott, R. Bassel-Duby, J.R. Sanes, and E.N. Olson. 2009. MicroRNA-206 delays ALS progression and promotes regeneration of neuromuscular synapses in mice. *Science*. 326:1549–1554. http://dx.doi.org/10.1126/science.1181046

Yadav, V.K., J.H. Ryu, N. Suda, K.F. Tanaka, J.A. Gingrich, G. Schütz, F.H. Glorieux, C.Y. Chiang, J.D. Zajac, K.L. Insogna, et al. 2008. Lrp5 controls bone formation by inhibiting serotonin synthesis in the duodenum. *Cell*. 135:825–837. http://dx.doi.org/10.1016/j.cell.2008.09.059

Yang, X., K. Matsuda, P. Bialek, S. Jacquot, H.C. Masuoka, T. Schinke, L. Li, S. Brancorsini, P. Sassone-Corsi, T.M. Townes, et al. 2004. ATF4 is a substrate of RSK2 and an essential regulator of osteoblast biology; implication for Coffin-Lowry Syndrome. *Cell*. 117:387–398. http://dx.doi.org/10.1016/S0092-8674(04)00344-7

Zhang, Y., R.L. Xie, C.M. Croce, J.L. Stein, J.B. Lian, A.J. van Wijnen, and G.S. Stein. 2011. A program of microRNAs controls osteogenic lineage progression by targeting transcription factor Runx2. *Proc. Natl. Acad. Sci. USA*. 108:9863–9868. http://dx.doi.org/10.1073/pnas.1018493108

Zhao, Y., E. Samal, and D. Srivastava. 2005. Serum response factor regulates a muscle-specific microRNA that targets Hand2 during cardiogenesis. *Nature*. 436:214–220. http://dx.doi.org/10.1038/nature03817